The Impact of Mutations on the Molecular Structure of the Cancer Biomarker X-linked Inhibitor of apoptosis protein (XIAP) and drug binding ensuring personalized drug selection

Tepap Zemnou Cromwel
EuroMed University of Fes (UEMF), Fes, MOROCCO
c.tepapzemnou@ueuromed.org

Abstract
The X-linked inhibitor of apoptosis protein (XIAP) inhibits caspases 3, 7 and 9, blocking apoptosis and promoting cancer development. Malfunctions of XIAP due to single nucleotide polymorphisms (SNPs) can cause X-linked lymphoproliferative syndrome type 2, an immunodeficiency. While several drugs targeting XIAP are in development, no in silico studies have evaluated the impact of SNPs on XIAP's molecular function and drug-binding affinity. This study uses computational methods to assess XIAP's molecular expression and prognostic value in various cancers and the effects of SNPs on XIAP's interactions with four inhibitors. Our findings show that XIAP is overexpressed in six cancers out of 33 examined in the GEPIA2 database. XIAP overexpression was correlated with cancer stages only in pancreatic adenocarcinoma (PAAD) and was linked to survival and prognosis in adrenocortical carcinoma (ACC), kidney renal clear cell carcinoma (KIRC) and oropharyngeal squamous cell carcinoma (OPSCC).

The study also revealed that SNPs can alter XIAP's structure, influencing patient responses to chemotherapy. Drugs with lower inhibitory capacity like GDC-0152 and TL32711 may be more effective for treating patients with these mutations. These findings emphasize the need for more research on XIAP genetic polymorphism to better determine its prognostic significance across cancers and to enhance precision medicine.

Keywords: Mutations, X-linked inhibitor of apoptosis protein, molecular docking, site-directed mutagenesis, *in silico*.

Introduction

Personalized medicine (PM), also known as precision medicine in oncology, is an innovative approach in treating and preventing cancer by considering genetic variability, the tumor environment and patients' lifestyles. This method aims to tailor therapies to the oncogenic factors of the tumor and modulate the immune environment to optimize tumor response while minimizing side effects, thus preserving patients' quality of life[1]. Furthermore, the vast amount of data generated from whole-genome sequencing often requires automated methods for annotating and prioritizing genetic variants[2]. Companion diagnostic tests can assess levels of proteins, genes, or specific mutations to identify an effective therapy tailored to an individual's condition[3].

Additionally, bioinformatics offers powerful and cost-effective techniques for profiling single nucleotide polymorphisms (SNPs) in a reduced timeline, revitalizing the field of personalized genomics[2]. Most of these techniques use sequence and/or structural data, along with the physicochemical properties of amino acid residues to classify variants as pathogenic, benign, or with uncertain significance. Understanding the three-dimensional (3D) structure of a target protein is crucial for determining the impact of a mutation on a specific disease, as it provides valuable insights into conformational changes of active sites induced by mutations and the protein's stability and flexibility[4].

Sequence alignment, *in silico* site-directed mutagenesis, molecular docking and molecular dynamics simulation can be used to map specific mutations and construct 3D models of the target protein by homology, allowing researchers to better understand the effect of a mutation on drug-target interaction and the relationship between drug response and protein structural variants[5]. The X-linked inhibitor of apoptosis protein (XIAP), also known as an inhibitor of apoptosis protein 3 (IAP3), baculoviral IAP repeat-containing protein 4 (BIRC4) and human IAP-like protein (hILP), is part of the IAP family first identified in insect baculovirus[6].

XIAP enzyme directly binds to BIR3 and BIR2 domains and inhibits the activation of effector caspases 9, 3 and 7 involved in both apoptotic pathways[7]. Cancer cells can resist drug-induced death due to faulty pro-apoptotic regulators or high levels of pro-survival proteins, causing chemotherapy failure. Neutralizing oncogenes can shorten chemotherapy and reduce drug doses. Targeting XIAP is a promising treatment approach for various cancers[8].

Antisense technology, SMAC/Diablo mimetics and siRNA have been used to lower XIAP overexpression, but antisense treatments were halted in phase I trials due to neurotoxicity. These methods aim to reduce XIAP mRNA, increasing apoptotic cell death of stem cells[9]. SMAC/Diablo mimetics, essential for neutralizing XIAP can lead to adverse effects

due to their higher binding affinity, as they are also able to bind BIR2 and BIR3 domains simultaneously. Developing antagonist molecules with lower micromolar affinity is necessary to reduce toxic effects[10,11]. To address this issue, numerous small molecules such as ASTX660, LCL161, GDC-0152 and TL32711 have been identified as effective inhibitors of the XIAP protein and have completed phases 1 and 2 of clinical trials[12–16]. Furthermore, research has shown that single nucleotide polymorphisms (SNPs) associated with mutations such as L307, E282Q, N340K and others in the BIRC4 gene can diminish the activity of the XIAP enzyme, leading to an immunodeficiency disease known as X-linked lymphoproliferative syndrome type 2 (XLP-2)[17].

XLP-2 typically presents in early life and is characterized by a high incidence of haemophagocytic lymphohistiocytosis (HLH), often triggered by Epstein-Barr virus infections, splenomegaly and inflammatory bowel disease (IBD), resulting in severe hyperinflammation and tissue damage[18]. However, the relationship between these XIAP mutations, the severity of cancer and the patient's response to cancer treatment or the treatment survival rate with these new small molecules remains unclear. Moreover, since increased binding of these antagonists in patients with XIAP mutations could exacerbate XLP-2, it is important to consider these mutations during the treatment. A comprehensive bioinformatic analysis of the XIAP gene could help also to better understand XIAP molecular function in different cancers and its value as a prognosis biomarker[19].

The results of such studies would enable clinicians to tailor treatments based on each patient's response to these molecules. Therefore, the main aim of this study is to use computational methods including bioinformatic analysis, *in silico* site-directed mutagenesis and molecular docking, to understand XIAP molecular expression and function in different cancers, how mutations affect the XIAP protein as a drug target, potentially resulting in varying binding affinities and interaction modes.

Material and Methods

XIAP differential gene expression analysis in different cancer types and stages: The GEPIA2 platform (http://gepia2.cancer-pku.cn/) was utilized to investigate XIAP expression levels across various cancers and their differential expression at different pathological stages. For differential gene expression analysis, the ANOVA statistical method was employed. We used log2(TPM + 1) transformed expression data for visualization, comparing TCGA tumors with normal TCGA tumors and GTEx normal tissues for paired normal data. The analysis parameters included a |log2FC| cutoff of 1 and a q-value cutoff of 0.01.

Investigation of the prognostic value of XIAP-related gene: The prognostic significance of the gene candidate was evaluated by analyzing the overall survival rate based on the OncoDB database (https://oncodb.org/index.html). The Log-rank test was employed for hypothesis testing, with a hazard ratio (HR) derived from the Cox proportional hazards model and a 95% confidence interval (CI) represented by a dotted line. A gene expression threshold of 50% (median value) was used to classify the samples into high-expression (cutoff-high) and low-expression (cutoff-low) cohorts. Samples with expression levels above 50% were assigned to the high-expression cohort, while those below 50% were placed in the low-expression cohort. A p-value of less than 0.05 was considered statistically significant.

Identification of XIAP co-expressed genes in different cancers: STRING database (http://string-db.org) was used to construct a protein-protein interaction (PPI) network and identify genes that interacted with the XIAP gene. Additionally, the GEPIA2 database was utilized to identify expressed genes in different cancers associated with XIAP. These overexpressed genes and XIAP-interacting genes were imported into a Venn Diagram (https://bioinformatics.psb.ugent.be/webtools/Venn/) for further analysis. The main genes co-expressed with XIAP in different cancers were identified based on the intersecting results.

Functional enrichment analysis: Gene Ontology (GO) and Kyoto Encyclopedia of Genes and Genomes (KEGG) Pathway Enrichment analyses based on these interacted genes were performed using the DAVID database (https://david.ncifcrf.gov/home.jsp). The GO enrichment analysis encompasses three main categories: biological process (BP), molecular function (MF) and cellular component (CC). KEGG pathway analysis was conducted to identify the potential signaling pathways of the overlapping co-expressed genes. The top 10 BP, CC, MF and KEGG pathways were selected with a P-value ≤ 0.05 and the results were visualized using SRplot (https://www.bioinformatics.com.cn/en).

***In silico* site-directed mutagenesis of XIAP**

Structural model of X-linked inhibitor of apoptosis protein (XIAP): The crystal structures of the Homo sapiens X-linked inhibitor of apoptosis protein without mutations (PDB ID: 5OQW; Resolution: 2.31 Å, R-Value Free: 0.246, R-Value Work: 0.213 and R-Value Observed: 0.215) in complex with the small molecules A4E or ASTX660, Zn2+ and Na+, were retrieved from the Protein Data Bank (https://www.rcsb.org/) to design the different mutants.

Identification and building of 3D models of XIAP variants: The Variant Viewer tool in UniProtKB/Swiss-Prot has helped to identify 370 variants linked to the Human E3 ubiquitin transferase XIAP (UniProtKB P98170)[20]. From these, three natural mutations E282Q, L307I and N340K were selected and a fourth mutation combining these three (E282QL307IN340K) was specifically generated for this study to examine a complex mutation (Table 1). The sequence of the XIAP protein (PDB ID: 5OQW) from the BIR3 domain and the Human E3 ubiquitin transferase XIAP (UniProt P98170) were aligned and annotated using

Geneious Prime (https://www.geneious.com/features/) to locate the mutation positions (Supplementary Figure S1). The 3D structures of the selected variants were created through *in silico* site-directed mutagenesis.

Human XIAP structures with different mutations were modeled using the "Build Mutant" protocol in the modeling environment of Discovery Studio Client v24.1 software (Figure 1). This protocol uses the Modeler program to mutate residues to specified types and optimize the conformation of mutated residues and their neighboring residues[21]. The rotamer with minimum energy and clashes has been chosen based on the "Search Side-Chain Rotamers tools" panel[22]. The resulting mutant models then underwent refinement of their geometry and energy minimization using default parameters of the "smart minimizer" algorithm, applying the CHARMM36 force field[23]. Discovery Studio Client v24.1 software addresses structural irregularities between the manually introduced mutations and their surroundings.

Molecular docking

Binding site identification: The most crucial aspect of molecular docking studies is the identification of active residues of the ligand binding pocket to generate the docking grid box. In this study, the selected PDB structure was XIAP (PDB ID: 5OQW) co-crystallized with the inhibitor A4E. The points and domain of active residues of the cavity of our target protein XIAP were identified based on protein-ligand interactions and data available on UniProtKB[24]. Additionally, the solvent-accessible area of the protein was calculated using the CASTp server. The CASTp web server is a simple and useful online tool for assessing the topology and pockets of sites within proteins[25].

Proteins preparation: To better understand the estimation of binding energy and binding mode between the different antagonists and target protein structures, *in silico* molecular docking has been performed using AutoDock 4[26]. The starting directory was set to a specific docking folder corresponding to XIAP protein wild type and variants. The processed protein molecules were imported into the Autodock 4 workspace. The missing atoms have been checked first of all and then repaired. The polar hydrogen was added and the Gasteiger and Kollman charges were calculated. Each protein was then used as a target after being stored in PDBQT format.

Table 1
Summary of the different selected dbSNP variants.
The first two columns represent the dbSNP accession number of the variants and the last two represent each amino acid of the enzyme replaced in the mutants by E (Glu) by Q (Gln), L (Leu) by I (Ile) and N (Asn) by K (Lys).

S.N.	Accession number	Amino acid position	Mutations
1	rs777303823	282	E>Q
2	rs1280883217	307	L>I
3	rs2053404854	340	N>K
4	/	282 307 340	E>Q L>I N>K

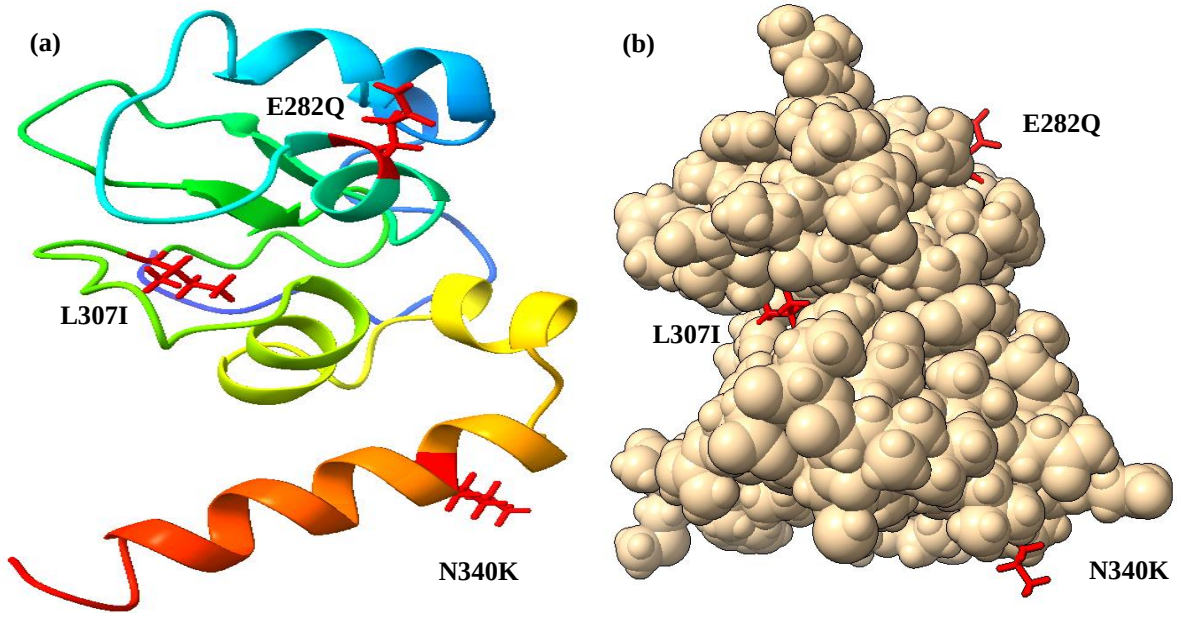

Figure 1: Representation of mutated Crystal Structure of X-linked inhibitor of apoptosis protein (PDB ID: 5OQW). a) Ribbons representation and b) Space-filling single-color representation. The different mutants are shown in red color.

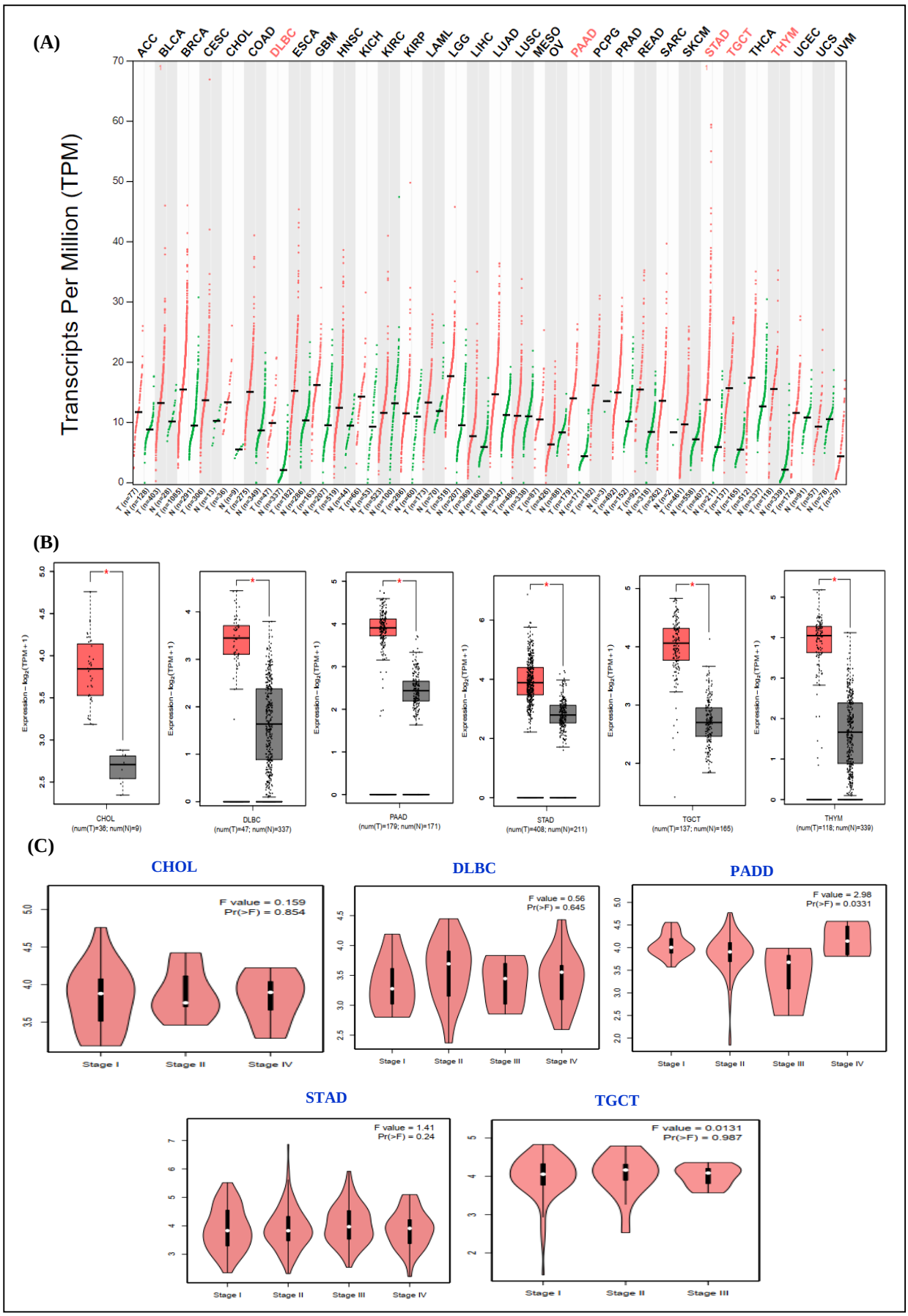

Figure 2: XIAP expression in different cancers and pathological stages. (A-B) XIAP gene overexpression showed in six cancer types (Red- and grey-colored boxes represent tumor and normal cells, respectively). (C) XIAP gene expression level correlation with pathological stages of cancers based on TCGA data.

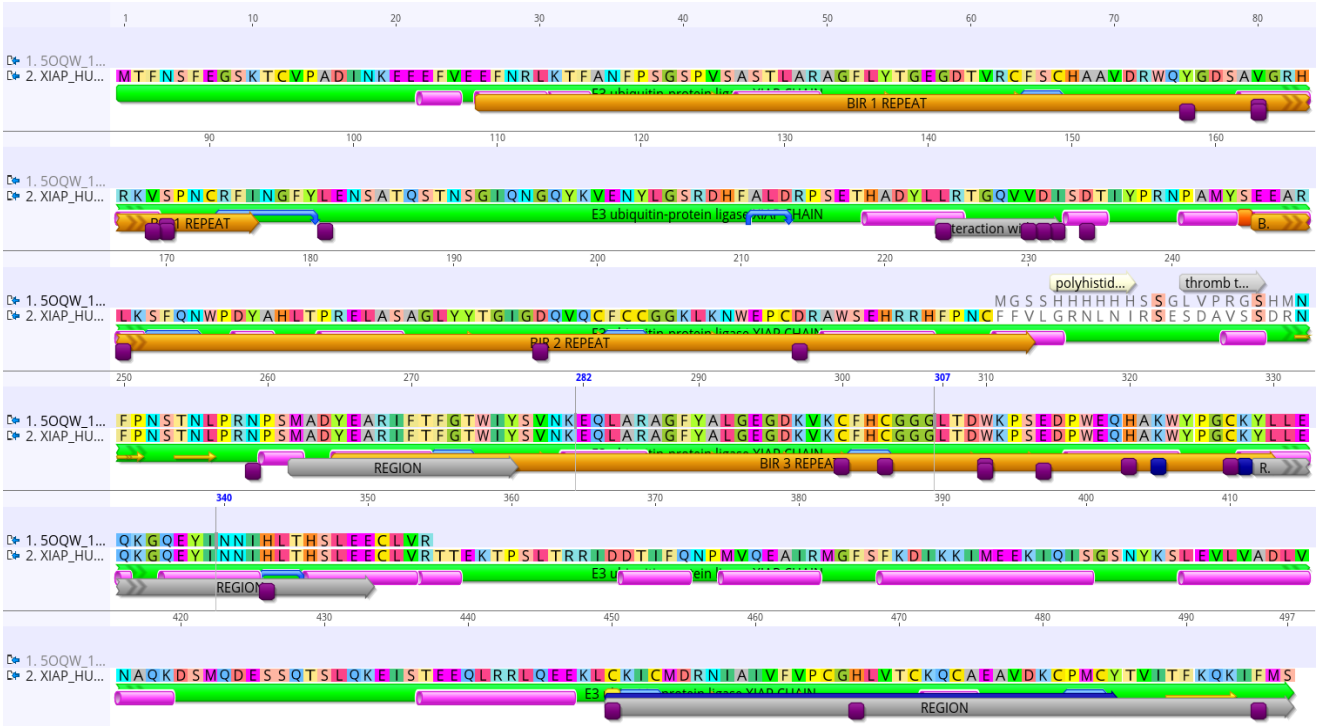

Figure S1: Alignment and annotation of primary amino acids sequences of the Human E3 ubiquitin transferase XIAP (P98170) and partial XIAP (5OQW). The highlighted position number in blue corresponds to amino acids E282, L307 and N340 selected for mutations. The region colored in orange (249-354) corresponds to the BIR 3 domain of XIAP protein (5OQW) while the green region (1-497) corresponds to the full Human E3 ubiquitin transferase XIAP

Ligands preparation: The structures of all four antagonists of XIAP were retrieved from the DrugBank databases, which provide information on chemical compounds such as structure, formula and pharmacological properties and their phase in clinical trials (https://go.drugbank.com/). The compounds namely ASTX660, GDC-0152, LCL-161 and TL32711 are drugs targeting XIAP protein which are currently completed clinical trials phase I or II**.** All of these structures were extracted in SDF and converted to protein data bank (PDB) format using the program Open Babel (https://sourceforge.net/projects/openbabel/files/openbabel/2.4.0/).

After all the ligands were imported into the Autodock 4 workspace, they were transformed into PDBQT format by selecting and detecting the root, choosing torsions and setting the number of torsions. The list of all the compounds, their DrugBank accession number, their clinical trials phase completed and 2D structures are given in supplementary table S1.

Docking process: After introducing the PDBQT files of each ligand with the respective proteins wild type XIAP and the four variants E282Q, L307I, N340K and E282QL307IN340K into the workspace for each docking simulation, the grid was meticulously designed to cover the active site, with an appropriate grid spacing of 0.375 Å. For each protein, the center grid box coordinates were set to x = 12.547, y = 69.911 and z = 21.196 and a grid size of 60× 60 × 60 Å along the x, y and z dimensions. Then, genetic algorithms were set to 300 population sizes, 27000 generations, 1000000 evaluations and 100 Genetic Algorithm (GA) runs to optimize docking results.

Finally, we docked the XIAP enzyme wild type and variants against the four antagonists and a post-docking analysis was performed to select the best binding poses. The resultant protein-ligand complexes were examined using the PLIP (Protein-Ligand Interaction Profiler) and Discovery Studio Client v21.1[27,28].

Results

XIAP overexpression analysis in different cancer types and pathological stages: Data extracted from the TCGA database revealed that XIAP expression was notably elevated in only 5 of the 33 cancer types examined (Figure 2A). We also assessed XIAP expression in normal tissues using RNA-sequencing data from the GTEx database. By comparing XIAP expression levels between cancers and their normal tissue counterparts, including GTEx data, we found that XIAP was upregulated in 6 cancers relative to normal tissues, as shown individually in boxplots in figure 2B. Additionally, we analyzed XIAP expression levels concerning cancer stages. A significant correlation was found between XIAP expression and the pathological stages of pancreatic adenocarcinoma (PAAD, p-value = 0.0331).

However, there was no significant correlation for cholangiocarcinoma (CHOL, p-value = 0.854), lymphoid neoplasm diffuses large B-cell lymphoma (DLBC, p-value = 0.645), stomach adenocarcinoma (STAD, p-value = 0.24), or testicular germ cell tumors (TGCT, p-value = 0.987) (Figure

2C). No data was available for thymoma (THYM) in the GEPIA database.

Role of XIAP overexpression in cancer prognosis: The overall survival time between cancers with higher XIAP expression and those with lower XIAP expression was compared across TCGA cancer types. The data revealed a significant correlation between high overall survival and poor prognosis in cancer patients with XIAP overexpression in three cancers among the 33 types analyzed in this work. These cancers include Adrenocortical carcinoma (ACC; p-value = 2.08e-03), kidney renal clear cell carcinoma (KIRC; p-value = 1.0e-03) and oropharyngeal squamous cell carcinoma (OPSCC; p-value = 1.5-e03).

Table S1
List of screened compounds in the current study along with their DrugBank accession number, clinical trial phase progression and 2D structures

DrugBank Accession	Compounds names	The clinical trial phase completed	2D Structures
DB16160	ASTX660	Phase I	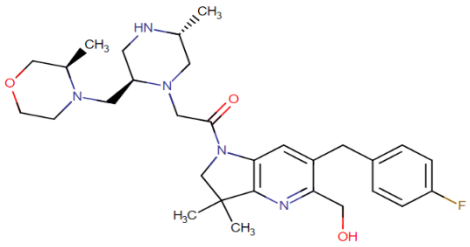
DB12380	GDC0152	Phase I	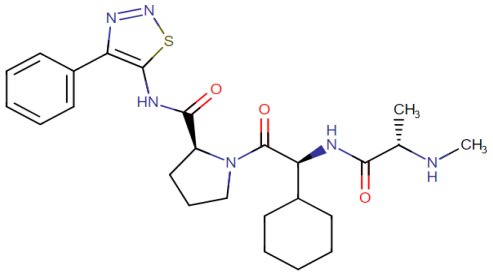
DB12085	LCL161	Phase II	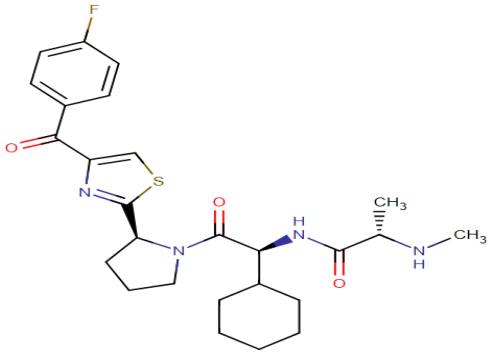
DB11782	TL32711	Phase II	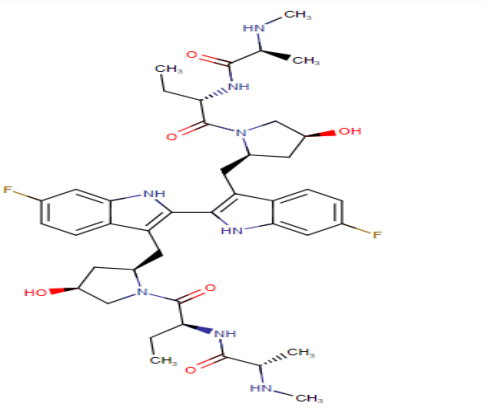

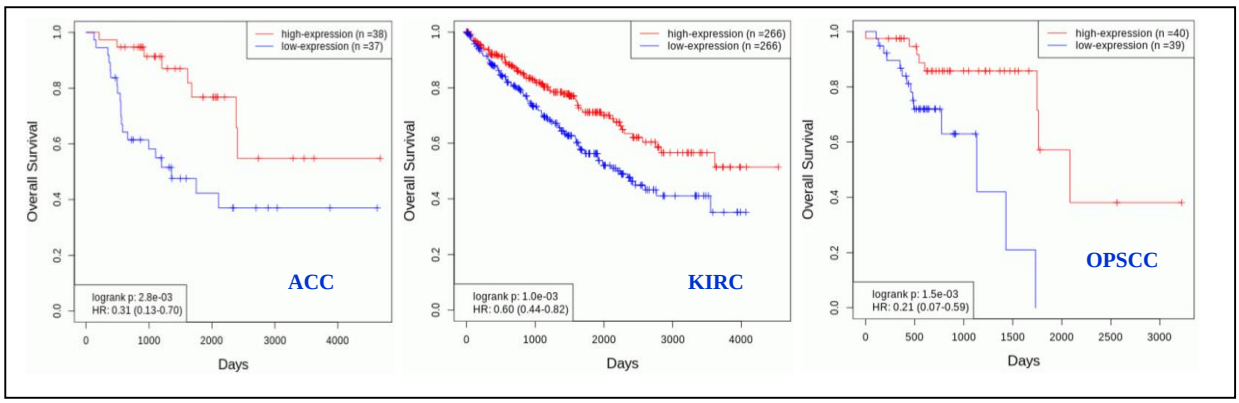

Figure 3: The correlation between XIAP gene expression and prognosis of patients with different cancers. There were significant correlation between upregulated gene expression, poor prognosis and Overall survival of patients with various tumours including ACC, KIRC and OPSCC.

Table S2
Interactions between residues of amino acids of KAT6A wild type and the three selected variants with different ligands.

Protein-Ligand	Residues	Distance (Å)	Bonds type
Wild type- ASTX660	Trp323	3.97	Pi-Alkyl
		4.52	Pi-Alkyl
		4.39	Pi-Alkyl
		5.10	Pi-Alkyl
		3.90	Pi-Sigma
	Tyr324	2.04	Conventional hydrogen bond
		4.07	Pi-Alkyl
	Trp310	4.95	Pi-Cation
		4.79	Pi-cation
	Val298	3.39	Fluorine
		3.02	Fluorine
	Lys297	3.39	Pi-Alkyl
	Lys299	5.48	Pi-Alkyl
	Leu292	5.46	Pi-Alkyl
	Gly306	2.84	Pi-Lone Pair
	Thr308	1.92	Conventional hydrogen bond
		1.83	Conventional hydrogen bond
	Leu307	4.23	Pi-Alkyl
	Asp309	2.98	Conventional hydrogen bond
		3.14	Carbon hydrogen bond
	Glu314	1.92	Salt Bridge
E282Q - ASTX660	Trp323	4.35	Pi-Alkyl
		5.05	Pi-Alkyl
		4.38	Pi-Alkyl
		3.88	Pi-Sigma
		3.97	Pi-Sigma
	Tyr324	2.09	Conventional hydrogen bond
		4.08	Pi-Alkyl
	Trp310	3.19	Pi-Sigma
	Lys322	2.67	Conventional hydrogen bond
	Val298	3.54	Fluorine
		2.69	Fluorine
	Lys297	4.09	Pi-Alkyl
	Lys299	5.18	Pi-Alkyl
	Gly306	2.88	Pi-Lone Pair

	Thr308	2.15	Conventional hydrogen bond
		1.75	Conventional hydrogen bond
	Leu307	4.56	Pi-Alkyl
	Asp309	2.67	Conventional hydrogen bond
		2.28	Conventional hydrogen bond
	Glu314	1.73	Salt Bridge
		2.85	Carbon hydrogen bond
	Gln319	3.79	Carbon hydrogen bond
L307I - ASTX660	Trp323	4.22	Pi-Alkyl
		4.96	Pi-Alkyl
		4.28	Pi-Alkyl
		4.94	Pi-Alkyl
		4.61	Pi-Alkyl
		3.78	Pi-Sigma
	Tyr324	4.31	Pi-Alkyl
		2.35	Conventional hydrogen bond
	Trp310	4.93	Pi-Cation
		4.97	Pi-Cation
	Gly306	2.96	Pi-Lone Pair
	Leu307	4.35	Alkyl
	Lys299	2.03	Conventional hydrogen bond
	Thr308	2.01	Conventional hydrogen bond
		1.77	Conventional hydrogen bond
	Glu314	1.77	Salt Bridge
N340K- ASTX660	Trp323	4.29	Pi-Alkyl
		4.39	Pi-Alkyl
		5.28	Pi-Alkyl
		4.93	Pi-Alkyl
		4.28	Pi-Alkyl
		3.80	Pi-Sigma
	Tyr324	4.00	Pi-Alkyl
	Trp310	3.42	Pi-Sigma
	Val298	3.98	Fluorine
	Lys297	3.94	Pi-Alkyl
	Thr308	2.14	Conventional hydrogen bond
		1.74	Conventional hydrogen bond
	Asp309	2.37	Conventional hydrogen bond
		2.28	Conventional hydrogen bond
	Glu314	2.02	Salt Bridge
E282QL307IN340K - ASTX660	Trp323	3.95	Pi-Alkyl
		4.99	Pi-Alkyl
		4.30	Pi-Alkyl
		4.17	Pi-Alkyl
		3.53	Pi-Sigma
	Tyr324	4.00	Pi-Alkyl
	Trp310	3.96	Pi-Sigma
	Val298	3.25	Fluorine
		2.71	Fluorine
	Lys297	4.33	Pi-Alkyl
	Thr308	1.83	Conventional hydrogen bond
	Ile307	1.74	Conventional hydrogen bond
		2.89	Carbon hydrogen bond
	Asp309	2.25	Conventional hydrogen bond
		5.15	Charge-Charge
	Glu314	3.20	Salt Bridge
Wild type- GDC0152	Trp323	4.24	Pi-Alkyl

		4.19	Pi-Alkyl
	Trp310	3.06	Pi-Alkyl
		3.77	Pi-Alkyl
	Lys297	4.05	Pi-Alkyl
		5.49	Pi-Alkyl
		3.48	Carbon hydrogen bond
	Asp309	3.74	Carbon hydrogen bond
	Thr308	1.85	Conventional hydrogen bond
		3.42	Pi-Sigma
	Leu307	5.13	Pi-Alkyl
E282Q - GDC0152	Trp323	4.63	Pi-Alkyl
		5.47	Pi-Alkyl
		5.01	Pi-Pi Stacked
	Tyr324	1.81	Conventional hydrogen bond
		5.48	Pi-Alkyl
	Trp310	5.42	Pi-Pi T-Shaped
		5.70	Pi-Pi T-Shaped
	Gly306	2.90	Carbon hydrogen bond
	Thr308	1.67	Conventional hydrogen bond
		2.94	Pi-Lone Pair
	Leu307	4.63	Pi-Alkyl
L307I - GDC0156	Trp323	4.00	Pi-Alkyl
		5.37	Pi-Alkyl
	Asp309	3.79	Carbon hydrogen bond
	Tyr324	1.81	Conventional hydrogen bond
		5.30	Pi-Sulfur
	Pro251	4.45	Pi-Alkyl
		3.59	Pi-Alkyl
	Thr308	1.94	Conventional hydrogen bond
		2.18	Conventional hydrogen bond
N340K- GDC0156	Trp323	5.29	Pi-Alkyl
	Tyr324	2.24	Conventional hydrogen bond
		2.73	Conventional hydrogen bond
	Pro251	4.23	Pi-Alkyl
	Thr308	2.94	Unfavorable Acceptor-acceptor
		2.08	Conventional hydrogen bond
E282QL307IN340K - GDC0152	Trp323	5.01	Pi-Alkyl
		4.46	Pi-Alkyl
		2.12	Conventional hydrogen bond
		2.24	Conventional hydrogen bond
	Lys299	2.98	Conventional hydrogen bond
	Lys332	2.90	Carbon hydrogen bond
	Tyr324	5.36	Pi-Alkyl
	Pro251	5.38	Pi-Alkyl
		4.77	Pi-Alkyl
Wild type- LCL161	Trp323	5.25	Pi-Alkyl
		4.45	Pi-Alkyl
		5.16	Pi-Alkyl
		3.17	Pi-Donor
		5.40	Pi-Sulfur
		4.96	Pi-Sulfur
		3.29	Pi-Sulfur
	Lys299	2.13	Conventional hydrogen bond
	Gly306	2.97	Pi-Donor hydrogen bond
	Thr308	2.65	Conventional hydrogen bond
		2.26	Conventional hydrogen bond

	Trp310	3.69	Pi-Sigma
	Gly304	3.34	Fluorine
E282Q - LCL161	Trp323	4.20	Pi-Pi Stacked
		3.38	Pi-Pi Stacked
		3.69	Pi-Sulfur
	Tyr324	4.60	Pi-Pi T-shaped
	Asn249	3.33	Fluorine
	Leu307	3.40	Alkyl
	Lys299	2.13	Conventional hydrogen bond
	Gly314	1.91	Conventional hydrogen bond
	Gln319	2.70	Conventional hydrogen bond
	Thr308	3.28	Carbon hydrogen bond
	Trp310	4.53	Pi-Alkyl
		4.85	Pi-Alkyl
L307I - LCL161	Trp323	4.18	Pi-Pi Stacked
		4.48	Pi-Pi Stacked
		2.01	Conventional hydrogen bond
		2.02	Conventional hydrogen bond
	Thr308	4.60	Fluorine
	Asp309	3.33	Fluorine
	Ile307	3.81	Pi-Sigma
N340K- LCL161	Trp323	4.62	Pi-Alkyl
		3.25	Pi-Donor hydrogen bond
		5.55	Pi-Sulfur
		5.93	Pi-Sulfur
	Tyr324	2.52	Conventional hydrogen bond
	Gly306	2.82	Pi-Donor hydrogen bond
	Lys299	2.05	Conventional hydrogen bond
	Thr308	2.01	Conventional hydrogen bond
	Trp310	43.90	Pi-Sigma
E282QL307IN340K - LCL161	Trp323	4.69	Pi-Alkyl
		2.87	Pi-Lone Pair
	Tyr324	4.65	Pi-Pi T-shaped
		2.53	Conventional hydrogen bond
	Glu314	3.25	Carbon hydrogen bond
	Gln319	3.50	Carbon hydrogen bond
	Thr308	2.13	Conventional hydrogen bond
	Pro251	5.24	Pi-Alkyl
	Pro325	4.47	Pi-Alkyl
Wild type- TL32711	Trp323	2.76	Conventional hydrogen bond
	Tyr324	5.14	Pi-Pi T-shaped
		2.73	Pi-Lone Pair
	Trp310	3.84	Pi-Sigma
	Thr308	3.10	Carbon hydrogen bond
		2.24	Conventional hydrogen bond
	Lys299	2.29	Conventional hydrogen bond
	Glu314	2.99	Conventional hydrogen bond
E282Q - TL32711	Trp323	2.45	Conventional hydrogen bond
		3.12	Carbon hydrogen bond
		5.42	Pi-Alkyl
		4.29	Pi-Alkyl

	Tyr324	2.50	Conventional hydrogen bond
	Gly306	2.99	Pi-Lone Pair
		3.85	Amide-Pi Stacked
		3.02	Amide-Pi Stacked
	Leu307	5.05	Pi-Alkyl
	Lys297	5.42	Pi-Alkyl
	Pro251	4.62	Pi-Alkyl
	Thr308	2.88	Pi-Donor hydrogen bond
L307I - TL32711	Trp323	3.21	Carbon hydrogen bond
	Ile307	4.67	Pi-Alkyl
	Tyr324	5.14	Pi-Alkyl
	Asn249	2.95	Conventional hydrogen bond
	Gly306	3.82	Amide-Pi Stacked
		3.26	Amide-Pi Stacked
	Leu307	5.05	Pi-Alkyl
	Thr308	3.34	Carbon hydrogen bond
		3.31	Fluorine
N340K- TL32711	Trp323	2.82	Conventional hydrogen bond
		3.67	Pi-Alkyl
		4.60	Pi-Alkyl
	Glu314	2.01	Conventional hydrogen bond
	Tyr324	2.50	Conventional hydrogen bond
	Leu307	3.35	Pi-Alkyl
	Thr308	2.69	Carbon hydrogen bond
		3.67	Fluorine
E282QL307IN340K - TL32711	Trp323	2.07	Conventional hydrogen bond
		2.61	Conventional hydrogen bond
		3.50	Pi-Sigma
	Gln319	3.48	Carbon hydrogen bond
	Tyr324	5.47	Pi-Alkyl
	Ile307	3.08	Fluorine
	Thr308	2.78	Conventional hydrogen bond
		3.92	Carbon hydrogen bond
	Gly306	3.33	Amide-Pi Stacked
		2.15	Conventional hydrogen bond
	Pro251	3.75	Pi-Alkyl

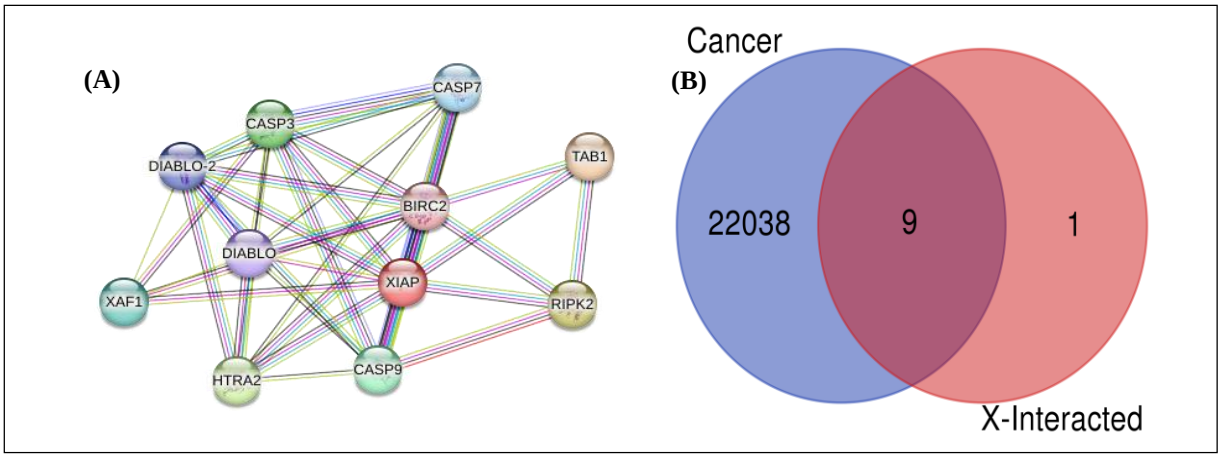

Figure 4: (A) Protein-protein interaction (PPI) of XIAP generated with STRING database. (B) Intersection analysis of Cancer genes (blue) and XIAP (red) interacted genes using Venn diagram.

Identification of XIAP co-expressed genes in different cancers: Using the STRING database, we constructed a network of 10 XIAP-binding protein interactions (Figure 4A). This network comprised of 11 nodes and 39 edges. Additionally, we retrieved 32,526 genes from the GEPIA2 database overexpressed in six cancers (CHOL, DLBC,

PAAD, STAD, TGCT and THYM). After removing duplicate genes, we obtained 22,038 unique genes.

The intersecting genes from the cancer-related genes and XIAP-interacted genes are shown in figure 4B, revealing that XAF1, CASP3, HTRA2, RIPK2, CASP7, TAB1, BIRC2, CASP9 and DIABLO are the common 9 genes interacting with XIAP in different cancers. The description of these nine genes is given in supplementary table S3.

Functional enrichment analysis: GO and KEGG pathway analyses were conducted for XIAP co-expressed genes to categorize their functions (Figure 5).

Table S3
Description of the nine intersecting genes retrieved from DAVID database.

Symbol	Type	Description
CASP9	Protein coding	Caspase 9
HTRA2	Protein coding	HtrA serine peptidase 2
CASP3	Protein coding	Caspase 3
RIPK2	Protein coding	receptor interacting serine/threonine kinase 2
CASP7	Protein coding	Caspase 7
BIRC2	Protein coding	Baculoviral IAP repeat containing 2
DIABLO	Protein coding	Diablo IAP-binding mitochondrial protein
XAF1	Protein coding	XIAP associated factor 1
TAB1	Protein coding	TGF-beta activated kinase 1 (MAP3K7) binding protein 1

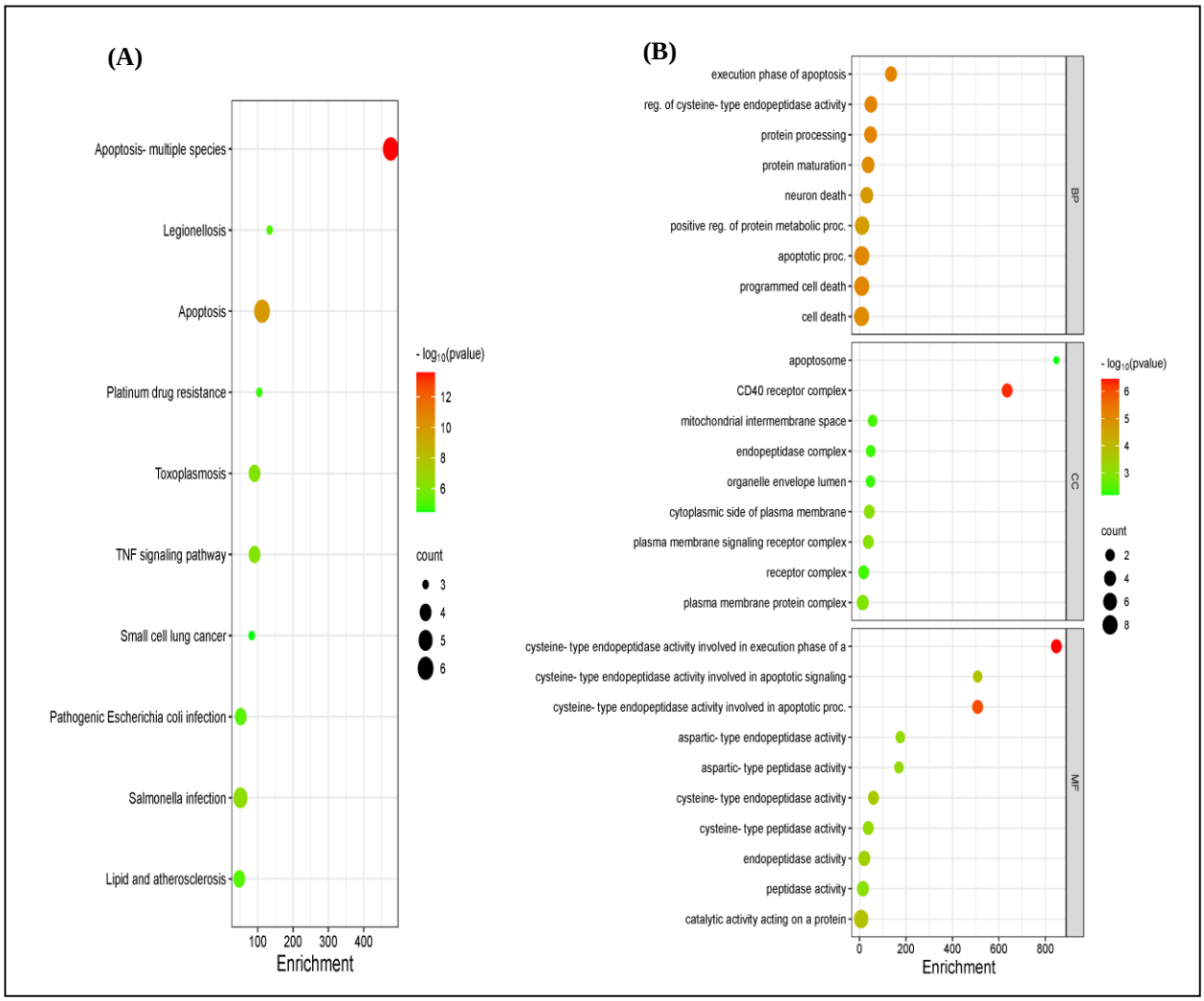

Figure 5: GO and KEGG analysis of XIAP co-expressed genes extracted from DAVID database. (A) The KEGG pathway analysis of XIAP co-expressed genes. (B) The GO enrichment analysis classified in terms of biological process (BP), cellular component (CC) and Molecular function (MF). The Y-axis corresponds to the different terms and the X-axis corresponds to the enrichment. The black circle specifies the number of gene per pathway.

GO analysis indicated that these intersecting genes were significantly enriched in the apoptotic process, programmed cell death and cell death within biological processes. Molecular function analysis revealed significant enrichment in endopeptidase activity, peptidase activity and catalytic activity acting on proteins. Cellular component analysis showed enrichment in the plasma membrane signaling receptor complex, receptor complex and plasma membrane protein complex. Additionally, KEGG pathway enrichment analysis demonstrated that the intersecting genes were particularly involved in apoptosis-multiple species, apoptosis, salmonella infection and TNF signaling pathways (Figure 5A). The main KEGG pathway, the apoptosis pathway is depicted in supplementary figure S2.

Binding site identification: The configuration of the XIAP structure, co-crystallized with A4E inhibitor and available on the PDB, was selected as the binding site. The binding position of the complex structure was retrieved so that the binding site could further be used during the molecular docking process. Based on the interaction pattern between XIAP and A4E (PDB ID: 5OQW), we have identified six Pi-Alkyl/Alkyl interactions formed with Tyr324, Trp323, Met248 and Lys297, four conventional hydrogen bonds formed residues Asp309 and Thr3058 and two carbon-hydrogen bonds formed with residue Gln319. We also observed one salt bridge established with residue Glu314 and one halogen interaction formed between the fluorine attached to the benzene ring and residue Val298 (see Supplementary Figure S3a). Analysis of the protein's solvent-accessible surface was conducted using the CastP server. The results showed that the protein has a total solvent-accessible surface of 172.919 $Å^2$ and a volume of 253.414 $Å^3$ for the predicted binding pocket. The solvent-accessible pocket of XIAP is illustrated in supplementary figure S3b.

Molecular docking analysis

Binding energy and protein-ligand interaction analysis: Molecular docking serves as a valuable tool for investigating the relationship between the structure and function of an enzyme, assessing its binding affinity to substrates and aiding in the drug design process by analyzing the potential of specific drugs to efficiently inhibit their target proteins. In this study, molecular docking was performed between four XIAP-related drugs and the wild-type protein, along with its four mutants (E282Q, L307I, N340K and E282QL307IN340K) generated using *in silico* site-directed mutagenesis to assess the impact of mutation on the molecular function of XIAP and drug binding. The ranking of protein-ligand complexes was based on docking scores (kcal/mol). The docking results are presented in table 2 while the interactions between the protein and ligands are further elucidated in figures 6, 7, 8 and 9, as well as in supplementary table S2.

In this investigation, ASTX660 showed a decreasing affinity from the wild-type protein to variants E282Q, L307I, N340K and E282QL307IN340K, with binding free energies of -12.79 kcal/mol, -12.55 kcal/mol, -11.22 kcal/mol, -10.40 kcal/mol and -8.33 kcal/mol respectively (Table 2). Detailed interaction analysis revealed five hydrogen bonds between ASTX660 and residues Tyr324, Thr308 and Asp309 of the wild-type protein, along with two Pi-cation interactions with Trp310 and one Pi-Lone pair with Gly306. ASTX660 was also engaged in ten hydrophobic interactions with residues Trp323, Tyr324, Lys297, Lys299, Leu307 and Lys292 and two fluorine interactions with Val298 and one salt bridge with Glu314. For the E282Q variant, ASTX660 maintained the same interactions but formed eight hydrogen bonds with Tyr324, Lys322, Thr308, Asp309, Glu314 and Gln319.

The L307I variant exhibited four hydrogen bonds with Tyr324, Lys299 and Thr308, two Pi-cation interactions with Trp310, one Pi-Lone pair with Gly306 and eight hydrophobic interactions with Trp323, Tyr324 and Leu307, along with a salt bridge with Glu314. In the N340K variant, ASTX660 formed four hydrogen bonds with Thr308 and Asp309, a salt bridge with Glu314, a fluorine interaction with Val298 and nine hydrophobic interactions with Trp323, Tyr324 and Lys297. For the E282QL307IN340K variant, ASTX660 formed four hydrogen bonds with Thr308, Ile307 and Asp309, a salt bridge with Glu314, eight hydrophobic interactions with Trp232, Tyr324, Trp310 and Lys297, two fluorine interactions with Val298 and one charge-charge interaction with Asp309 (Figure 6a, 6c and Supplementary Table S2).

The inhibitor GDC0152 showed strong binding potential with the wild-type protein and variants E282Q, L307I, N340K and E282QL307IN340K, with binding energies of -9.17 kcal/mol, -8.70 kcal/mol, -7.67 kcal/mol, -8.30 kcal/mol and -7.65 kcal/mol respectively (Table 2). Interaction analysis indicated that GDC0152 formed three hydrogen bonds with Lys297, Asp309 and Thr308 and eight hydrophobic interactions with Trp323, Trp310, Thr308, Leu307 and Lys297 in the wild-type XIAP protein.

For the E282Q variant, it formed three hydrogen bonds with Tyr324, Gly306 and Thr308, one Pi-lone pair interaction with Thr308 and seven hydrophobic interactions with Trp323, Tyr324, Trp310 and Leu307. In the L307I variant, GDC0152 established four hydrogen bonds with Asp309, Tyr324 and Thr308, one Pi-sulfur interaction with Tyr324 and four Pi-alkyl interactions with Trp323 and Pro251. For the N340K variant, it formed three hydrogen bonds with Tyr324 and Thr308, two Pi-alkyl interactions with Trp323 and Pro251 and one unfavorable bond with Thr308. The E282QL307IN340K variant showed four hydrogen bonds with Trp323, Lys299 and Lys332 and five Pi-alkyl interactions with Trp323, Tyr324 and Pro251 (Figure 7a, 7c and Supplementary Table S2).

LCL161 displayed notable binding potential to the wild-type and the variants E282Q, L307I, N340K and E282QL307IN340K with binding energies of -8.11

kcal/mol, -7.61 kcal/mol, -7.27 kcal/mol, -8.39 kcal/mol and -7.85 kcal/mol respectively (Table 2). The wild-type interactions included four hydrogen bonds with Lys299, Gly306 and Thr308, five hydrophobic interactions with Trp323 and Trp310, three Pi-sulfur interactions with Gly304 and one fluorine interaction with Trp323. For the E282Q variant, LCL161 engaged in four hydrogen bonds with Lys299, Gly314, Gln319 and Thr308, six hydrophobic interactions with Trp323, Tyr324, Leu307 and Trp310 and one fluorine interaction with Asn249.

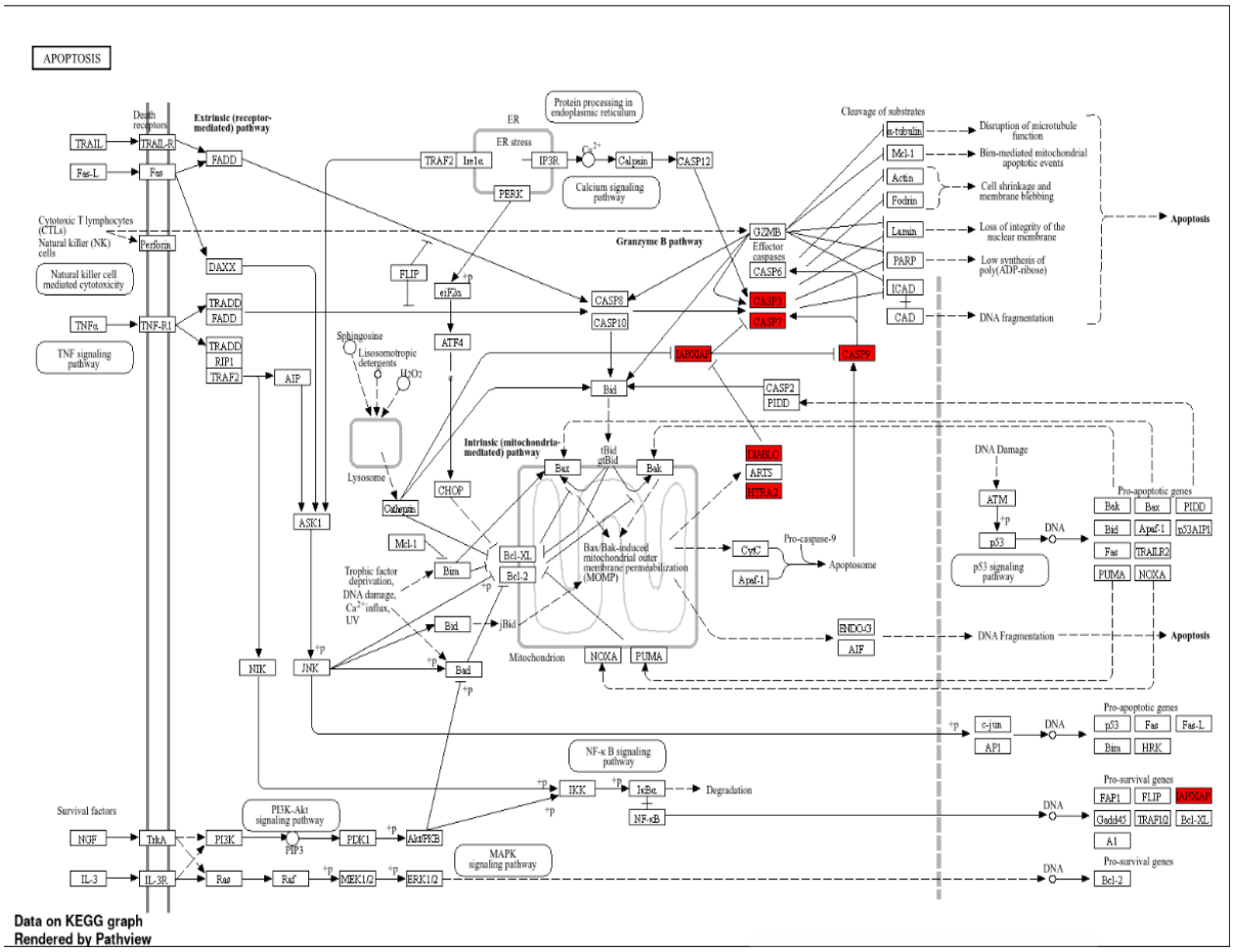

Figure S2: Apoptosis signaling pathways. Red stars indicate our identified XIAP co-expressed genes.

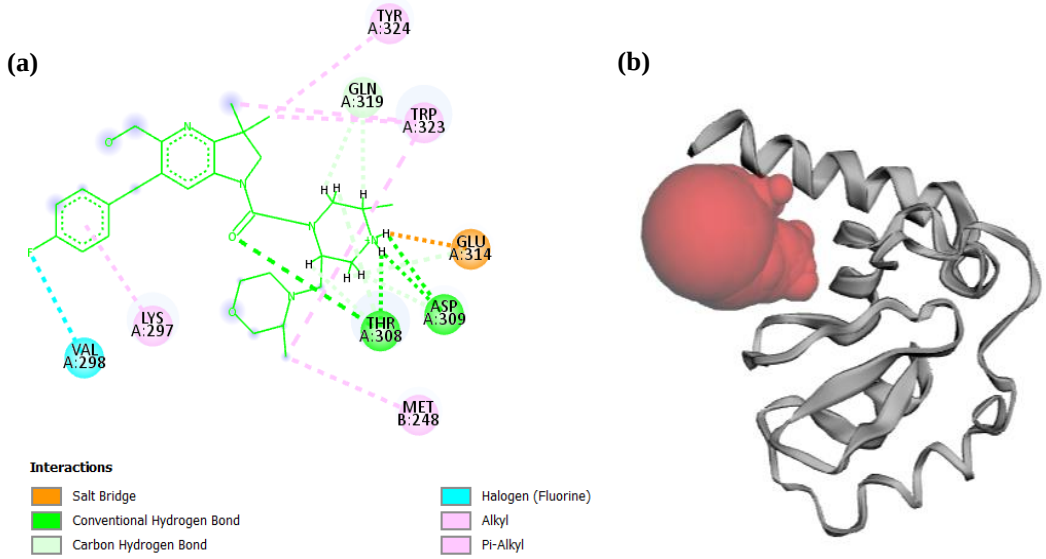

Figure S3: (a) Depicted 2D figure showing the binding site of XIAP protein complexed with the selected ligand (PDB ID: 5OQW). The different interactions are highlighted in color with their respective amino acids. (b) A Solvent accessible surface area of the binding cavity of XIAP.

Table 2
Binding energy values from molecular docking of different ligands with KAT6A enzyme.

Compounds	DrugBank Accession Number	Molecular docking results (kcal/mol)				
		Wild type	E282Q	L307I	N340K	E282QL307IN340K
ASTX660	DB16160	-12.79	-12.55	-11.22	-10.40	-8.83
GDC0152	DB12380	-9.17	-8.70	-7.67	-8.30	-7.65
LCL161	DB12085	-8.11	-7.61	-7.27	-8.39	7.85
TL32711	DB11782	-5.69	-4.56	-5.81	-3.23	-5.40

In the L307I variant, Trp323 formed two hydrogen bonds with LCL161, Thr308 and Asp309 formed two fluorine interactions and Trp323 and Ile307 were involved in two hydrophobic interactions. For the N340K variant, LCL161 formed five hydrogen bonds with Tyr324, Lys299, Trp323, Gly306 and Thr308 and two hydrophobic interactions with Trp323 and Trp310. The E282QL307IN340K variant established two Pi-sulfur interactions with Trp323 (Figure 8a, 8c and Supplementary Table S2).

The compound TL32711 showed binding energies of -5.69 kcal/mol, -4.56 kcal/mol, -5.81 kcal/mol, -3.23 kcal/mol and -5.40 kcal/mol for the wild-type protein and the variants E282Q, L307I, N340K and E282QL307IN340K respectively (Table 2). For the wild-type protein, TL32711 formed five hydrogen bonds with Trp323, Thr308, Lys299 and Glu314, along with two hydrophobic interactions and one Pi-lone pair interaction with Trp310 and Tyr324. In the E282Q variant, TL32711 formed four hydrogen bonds with Trp323, Tyr324 and Thr308, four alkyl interactions with Trp323, Gly306, Leu307, Lys297 and Pro251 and one Pi-lone pair interaction with Gly306.

For the L307I variant, TL32711 established three hydrogen bonds with Trp323, Asn249 and Thr308, five hydrophobic interactions and one fluorine interaction with Ile307, Tyr324, Gly306, Leu307 and Thr308. For the N340K variant, four hydrogen bonds were identified with Trp323, Glu314, Tyr324 and Thr308, three Pi-alkyl interactions with Trp323 and Leu307 and one fluorine interaction with Thr308. The E282QL307IN340K variant showed six hydrogen bonds with Trp323, Gln319, Thr308 and Gly306, four hydrophobic interactions with Trp323, Tyr324, Gly306, Pro251 and Ile307 and one fluorine interaction (Figure 9a, 9c and Supplementary Table S2).

Binding site conformation and binding mode analysis: The wild-type protein XIAP and the four variants were also investigated in changes in the conformational state of their binding site and catalysis. Figures 6b, 7b, 8b and 9b revealed that these mutations can alter the XIAP enzyme as well as its binding site conformation which can result in divergence in binding affinities of different drugs, in variation of protein-ligands interactions and their respective distances and consequently the binding mode of the drug at the active cavity. However, we observed also that all four drugs interacted with at least three amino acid residues of the predicted binding site. According to the observations, the high number of mutations is associated with a significant disorganization of the binding site conformation and consequently with a significant decrease in binding affinity (Table 2).

Discussion

Despite significant advances in understanding cancer biology, current therapeutic approaches are guided not only by molecular profiling, which categorizes tumors based on certain biomarkers but also by single nucleotide polymorphisms (SNPs). SNPs are valued not only as markers for constructing genetic maps but also as potential functional polymorphic variants directly involved in complex diseases like cancer and drug response[2,29]. The past decade has seen a substantial increase in studies aiming to comprehensively understand the genetic basis of interindividual variability in drug response[5,30]. Understanding the processes underpinning phenotypic variability in drug response at the protein level is crucial for the development of personalized medicine [31].

XIAP is a protein that has been very attractive as a target and prognostic biomarker in cancer therapy. However, the impact of XIAP polymorphism on cancer treatment is not yet understood. Therefore, for this study, we first investigate the molecular function and prognostic value of XIAP in different cancers using a comprehensive bioinformatic analysis. The gene expression analysis results revealed that among the 33 types of cancers present in the GEPIA2 database, XIAP is upregulated in six cancers namely CHOL, DBLC, PAAD, STAD, TGCT and THYM.

The overexpression analysis of the XIAP gene in different cancer pathological stages revealed a significant correlation between XIAP overexpression and the pathological stages of only one of the six cancers, pancreatic adenocarcinoma (PAAD, p-value = 0.0331). Adding to this, the prognostic value of XIAP expression has been also investigated. It has shown a significant correlation between overexpression of XIAP and overall survival in three cancers including ACC, KIRC and OPSCC.

It has been reported that one of the defining characteristics of cancer is the ability of cancer cells to evade apoptosis which then contributes to cell proliferation, metastasis and therapeutic resistance. That is why inhibitors of apoptosis proteins such as XIAP have gained past years as potential targets for developing new cancer therapies[10].

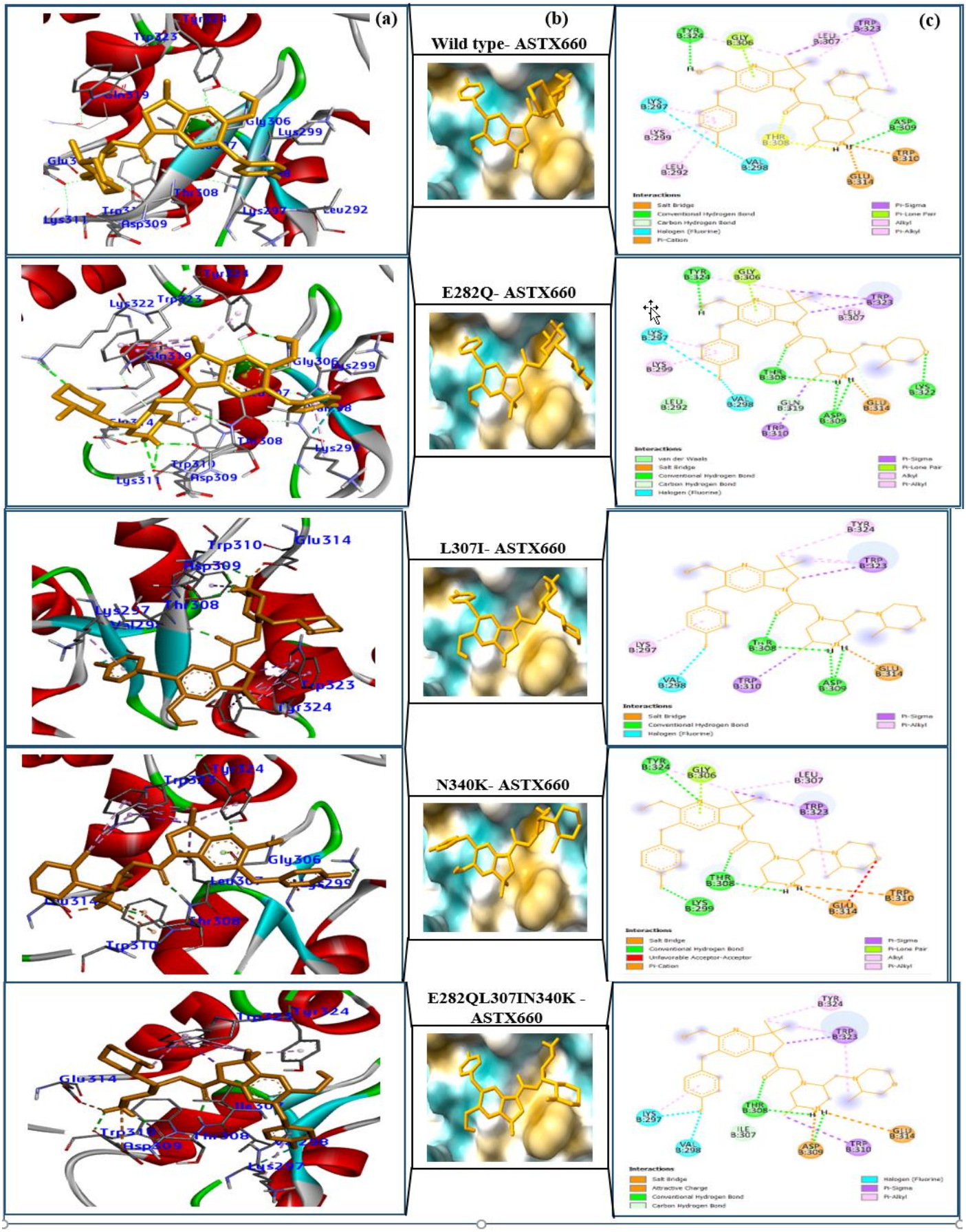

Figure 6: Protein-ligands interactions of XIAP wild type and variants with ASTX660. (a) 3D receptor-ligand and (c) 2D receptor-ligand interactions. (b) The conformational state of the binding site of the wild-type protein and variants upon fixation of ASTX660

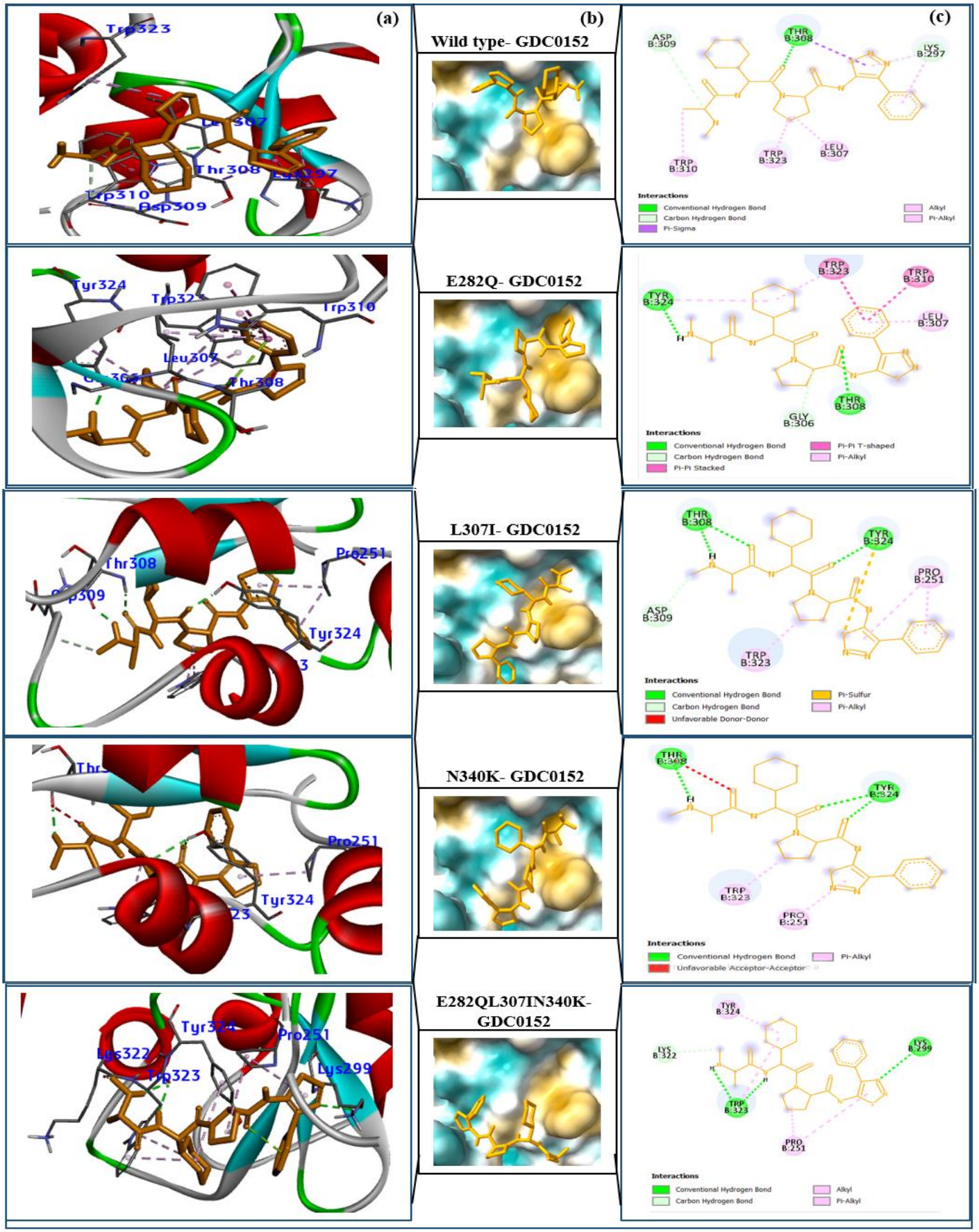

Figure 7: Protein-ligands interactions of XIAP wild type and variants with GDC0152. (a) 3D receptor-ligand and (c) 2D receptor-ligand interactions. (b) The conformational state of the binding site of the wild-type protein and variants upon fixation of GDC0152.

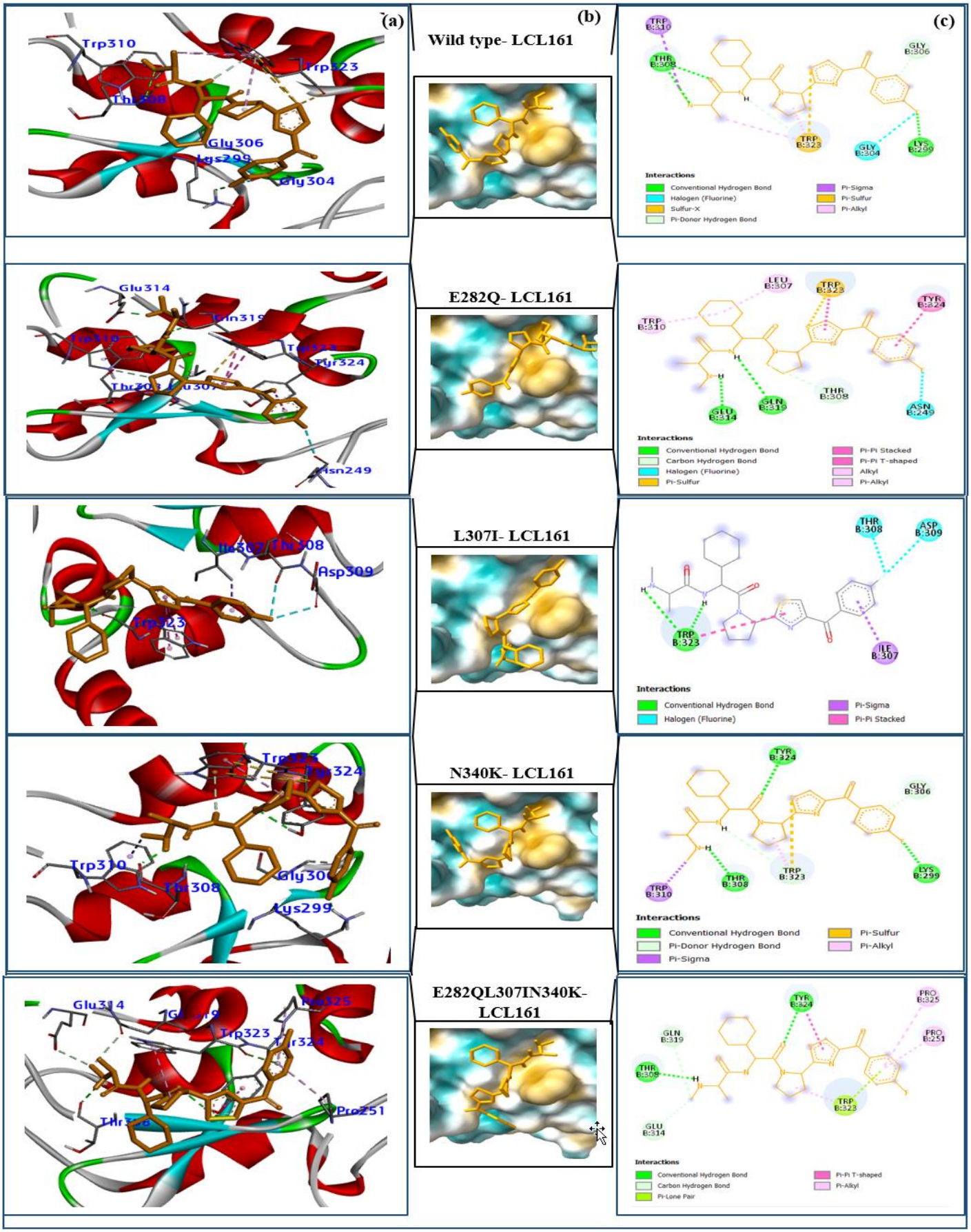

Figure 8: Protein-ligands interactions of XIAP wild type and variants with LCL161. (a) 3D receptor-ligand and (c) 2D receptor-ligand interactions. (b) The conformational state of the binding site of the wild-type protein and variants upon fixation of LCL161

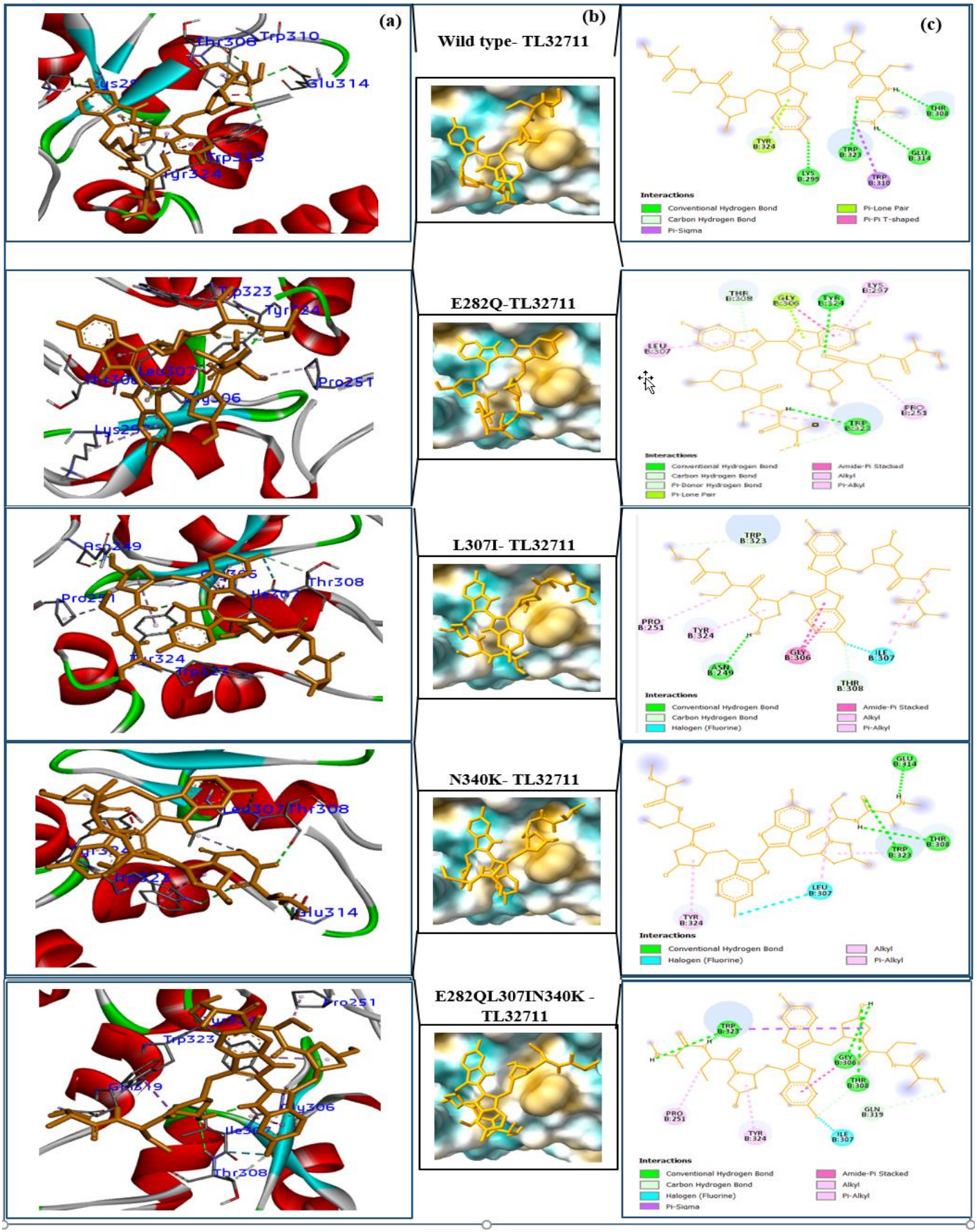

Figure 9: Protein-ligands interactions of XIAP wild type and variants with TL32711. (a) 3D receptor-ligand and (c) 2D receptor-ligand interactions. (b) The conformational state of the binding site of the wild-type protein and variants upon fixation of TL32711.

Our previous results support that XIAP upregulation could be beneficial for cancer patients, as they confirmed the prognostic value of XIAP enzyme in pan-cancer. Furthermore, many inhibitors able to target XIAP and increase prognosis and overall survival in cancer patients have been discovered and have completed phases 1 and 2 of clinical trials[12–16].

GO and KEGG pathways enrichment analysis revealed the mechanism by which XIAP induces cancer cell proliferation. All the results converge mostly on apoptosis, programmed cell death and TNF signaling pathways (Figure 5 and Supplementary Figure S3). Carcinogenesis is a complex multistep process in which a single cell transforms into a tumor and metastasizes to other sites. Apoptosis, an essential mechanism, maintains the balance between cell survival and death, thus preventing cancer and associated diseases. This process is divided into intrinsic and extrinsic pathways, both converging towards the execution pathway.

The key components include initiator caspases (caspase-8 and caspase-9), SMAC/DIABLO (Second Mitochondrial Activator of Caspases/Direct IAP Binding Protein) and executioner caspases (caspase-3, caspase-6, caspase-7 and caspase-10)[32]. XIAP enzyme can inhibit the activation of effector caspases 9, 3 and 7 to block apoptosis. To prevent this, SMAC/DIABLO can naturally counteract XIAP, resulting in caspase activation and the promotion of programmed cell death under normal conditions[33].

For the next step of our work, we identified three SNPs from the SNP database namely E282Q, L307I and N340K (Table 1) which have been described as missense mutations and are associated with a decrease in XIAP enzyme activity leading to an immunodeficiency disease known as X-linked lymphoproliferative syndrome type 2 (XLP-2)[17]. Based on this, *in silico* site-directed mutagenesis has been used to generate the three corresponding variants. We also generated a fourth variant namely E282QL307IN340K, which combined the three previous ones to simulate the context of complex mutations, as it has been shown that some patient's genes can be submitted to multiple mutations for XIAP enzymes[34]. Then, molecular docking was carried between the different variants and wild-type XIAP and four antagonists namely ASTX660, LCL161, GDC-0152 and TL32711.

The docking results generally indicated that ASTX660 is the most effective of the four drugs, showing the highest affinity with both the wild-type XIAP and its four variants. We observed a gradual reduction in binding affinity for all the drugs with the mutations, except for LCL161-N340K and TL32711-L307I, where the binding affinity increased slightly but not significantly. The complex mutation E282QL307IN340K caused the most significant reduction in binding energy for all four drugs, likely because complex mutations significantly alter the target protein more than simple mutations. Notably, the TL32711-N340K result had the lowest binding energy at 3.23 kcal/mol. Additionally, the results showed variations in the binding site conformation, which could lead to differences in binding modes, protein-ligand interactions and the distances between each drug and the different protein structures. This suggests that mutations can alter the structure and molecular function of the XIAP protein, resulting in variability in binding affinities and protein-ligand interactions. It has been shown that these mutations alter the BIRC4 gene in humans, decreasing the activity of the XIAP protein[34] and in the case of cancer treatment, this could also lead to variable drug responses associated with protein structural variants. Previous studies reported also that SNPs can alter protein structure by disrupting directly the ligand interaction sites[35,36]. As these mutations induce XIAP deficiency or reduce its activity, leading to an immunodeficiency XLP-2, it can result in hyperinflammation and tissue damage in patients[34].

The treatment of cancer patients with XLP-2 needs to be done carefully and with weak inhibitors of XIAP enzyme to limit not only the side effects of XLP-2. It is proved that some mutations can cause a severe inhibition of XIAP protein expression by creating a premature stop codon in the XIAP gene and enhancing the clinical manifestation of XLP-2[18]. Our findings suggest that these drugs could be used to treat cancer patients with XIAP deficiencies, as we observed a reduced affinity of these compounds for different XIAP variants. An inhibitor with a high binding affinity can significantly reduce an enzyme's activity compared to an inhibitor with a lower binding affinity. For treating cancer patients without defective XIAP function, ASTX660 is the most effective, followed by GDC-0152.

However, for patients with XIAP deficiencies, weaker inhibitors like LCL161 and TL32711 may be more appropriate, as they will not significantly reduce or abolish XIAP protein expression. Since these drugs have completed their first phase of clinical trials, it is important to sequence and characterize the XIAP gene of each patient before starting treatment, as different mutations cause varying severities of XIAP dysfunction. The binding affinities, particularly for TL32711-N340K, indicate that XIAP mutations can induce resistance to cancer treatments with these small molecules, as the affinity is too low.

Conclusion

In this *in silico* study, we analyzed the expression levels of XIAP across various cancer types and pathological stages, also investigating its prognostic value in cancer therapy using bioinformatic tools. The results indicated that XIAP is upregulated in only six cancers and can be used as a prognostic biomarker in different cancers. Additionally, we conducted molecular docking of wild-type XIAP and four structural variants (E282Q, L307I, N340K and E282QL307IN340K) with four developmental drugs: ASTX660, LCL161, GDC-0152 and TL32711 to evaluate the impact of mutations on XIAP and its drug binding.

The docking analysis revealed that these mutations altered the structure and molecular function of XIAP, disrupted the binding site and led to variability in protein-ligand interactions, reducing the binding affinity of the four drugs. These findings suggest that sequencing and characterizing the XIAP gene for mutations in cancer patients are crucial before commencing treatment with these drugs to ensure efficacy and safety. This is particularly important since these mutations can also cause the immunodeficiency XLP-2, which can severely impact the patient's life. We anticipate that our computational findings on XIAP, once validated, will significantly contribute to characterize the prognostic value of XIAP in different cancers, understanding individual drug responses and enhancing precision medicine in oncology.

Acknowledgement

The authors thank the EuroMed University of Fes for providing the facilities necessary to carry out this work.

References

1. Adasme M.F., Linnemann K.L., Bolz S.N., Kaiser F., Salentin S., Haupt V.J. and Schroeder M., PLIP 2021: expanding the scope of the protein-ligand interaction profiler to DNA and RNA, *Nucleic Acids Research*, **49**, W530–W534 **(2021)**

2. Ardecky R.J., Welsh K., Finlay D., Lee P.S., González-López M., Ganji S.R., Ravanan P., Mace P.D., Riedl S.J., Vuori K., Reed J.C. and Cosford N.D.P., Design, synthesis and evaluation of inhibitor of apoptosis protein (IAP) antagonists that are highly selective for the BIR2 domain of XIAP, *Bioorganic & Medicinal Chemistry Letters*, **23**, 4253 **(2013)**

3. Benetatos C.A., Mitsuuchi Y., Burns J.M., Neiman E.M., Condon S.M., Yu G., Seipel M.E., Kapoor G.S., LaPorte M.G., Rippin S.R., Deng Y., Hendi M.S., Tirunahari P.K., Lee Y.H., Haimowitz T., Alexander M.D., Graham M.A., Weng D., Shi Y., McKinlay M.A. and Chunduru S.K., Birinapant (TL32711), a Bivalent SMAC Mimetic, Targets TRAF2-Associated cIAPs, Abrogates TNF-Induced NF-κB Activation and Is Active in Patient-Derived Xenograft Models, *Molecular Cancer Therapeutics*, **13**, 867–879 **(2014)**

4. Bohl C.E., Wu Z., Miller D.D., Bell C.E. and Dalton J.T., Crystal Structure of the T877A Human Androgen Receptor Ligand-binding Domain Complexed to Cyproterone Acetate Provides Insight for Ligand-induced Conformational Changes and Structure-based Drug Design, *Journal of Biological Chemistry*, **282**, 13648–13655 **(2007)**

5. Boutet E., Lieberherr D., Tognolli M., Schneider M., Bansal P., Bridge A.J., Poux S., Bougueleret L. and Xenarios I., UniProtKB/ Swiss-Prot, the Manually Annotated Section of the UniProt KnowledgeBase: How to Use the Entry View, *Methods in Molecular Biology*, **1374**, 23–54 **(2016)**

6. Cetraro P., Plaza-Diaz J., MacKenzie A. and Abadía-Molina F., A Review of the Current Impact of Inhibitors of Apoptosis Proteins and Their Repression in Cancer, *Cancers*, **14**, 1671 **(2022)**

7. Daly A.K., Pharmacogenetics and human genetic polymorphisms, *Biochemical Journal*, **429**, 435–449 **(2010)**

8. Devi G.R., Finetti P., Morse M.A., Lee S., de Nonneville A., Van Laere S., Troy J., Geradts J., McCall S. and Bertucci F., Expression of X-Linked Inhibitor of Apoptosis Protein (XIAP) in Breast Cancer Is Associated with Shorter Survival and Resistance to Chemotherapy, *Cancers*, **13**, 2807 **(2021)**

9. Duckett C.S., Nava V.E., Gedrich R.W., Clem R.J., Van Dongen J.L., Gilfillan M.C., Shiels H., Hardwick J.M. and Thompson C.B., A conserved family of cellular genes related to the baculovirus iap gene and encoding apoptosis inhibitors, *EMBO Journal*, **15**, 2685–2694 **(1996)**

10. Fadó R., Moubarak R.S., Miñano-Molina A.J., Barneda-Zahonero B., Valero J., Saura C.A., Moran J., Comella J.X. and Rodríguez-Álvarez J., X-linked inhibitor of apoptosis protein negatively regulates neuronal differentiation through interaction with cRAF and Trk, *Scientific Reports*, **3**, 2397 **(2013)**

11. Fernald G.H., Capriotti E., Daneshjou R., Karczewski K.J. and Altman R.B., Bioinformatics challenges for personalized medicine, *Bioinformatics*, **27**, 1741–1748 **(2011)**

12. Hoeben A., Joosten E.A.J. and van den Beuken-van Everdingen M.H.J., Personalized Medicine: Recent Progress in Cancer Therapy, *Cancers*, **13**, 242 **(2021)**

13. Hu R., Li J., Liu Z., Miao M. and Yao K., GDC-0152 induces apoptosis through down-regulation of IAPs in human leukemia cells and inhibition of PI3K/Akt signaling pathway, *Tumor Biology*, **36**, 577–584 **(2015)**

14. Jan R. and Chaudhry G.S., Understanding Apoptosis and Apoptotic Pathways Targeted Cancer Therapeutics, *Advanced Pharmaceutical Bulletin*, **9**, 205–218 **(2019)**

15. Kalathiya U., Padariya M. and Baginski M., Structural, functional and stability change predictions in human telomerase upon specific point mutations, *Scientific Reports*, **9**, 8707 **(2019)**

16. Kester R.F., Donnell A.F., Lou Y., Remiszewski S.W., Lombardo L.J., Chen S., Le N.T., Lo J., Moliterni J.A., Han X., Hogg J.H., Liang W., Michoud C., Rupert K.C., Mischke S., Le K., Weisel M., Janson C.A., Lukacs C.M., Fretland A.J., Hong K., Polonskaia A., Gao L., Li S., Solis D.S., Aguilar D., Tardell C., Dvorozniak M., Tannu S., Lee E.C., Schutt A.D. and Goggin B., Optimization of benzodiazepinones as selective inhibitors of the X-linked inhibitor of apoptosis protein (XIAP) second baculovirus IAP repeat (BIR2) domain, *Journal of Medicinal Chemistry*, **56**, 7788–7803 **(2013)**

17. Krzyszczyk P., Acevedo A., Davidoff E.J., Timmins L.M., Marrero-Berrios I., Patel M., White C., Lowe C., Sherba J.J., Hartmanshenn C., O'Neill K.M., Balter M.L., Fritz Z.R., Androulakis I.P., Schloss R.S. and Yarmush M.L., The growing role of precision and personalized medicine for cancer treatment, *Technology*, **6**, 79–100 **(2018)**

18. Lahti J.L., Tang G.W., Capriotti E., Liu T. and Altman R.B., Bioinformatics and variability in drug response: a protein structural perspective, *Journal of the Royal Society Interface*, **9**, 1409–1437 **(2012)**

19. Lukacs C., Belunis C., Crowther R., Danho W., Gao L., Goggin B., Janson C.A., Li S., Remiszewski S., Schutt A., Thakur M.K.,

Singh S.K., Swaminathan S., Pandey R., Tyagi R., Gosu R., Kamath A.V. and Kuglstatter A., The structure of XIAP BIR2: understanding the selectivity of the BIR domains, *Acta Crystallographica Section D: Biological Crystallography*, **69**, 1717–1725 **(2013)**

20. Mita M.M., LoRusso P.M., Papadopoulos K.P., Gordon M.S., Mita A.C., Ferraldeschi R., Keer H., Oganesian A., Su X.Y., Jueliger S. and Tolcher A.W., A Phase I Study of ASTX660, an Antagonist of Inhibitors of Apoptosis Proteins, in Adults with Advanced Cancers or Lymphoma, *Clinical Cancer Research*, **26**, 2819–2826 **(2020)**

21. Momany F.A. and Rone R., Validation of the general purpose QUANTA® 3.2/CHARMm® force field, *Journal of Computational Chemistry*, **13**, 888–900 **(1992)**

22. Morris G.M., Huey R., Lindstrom W., Sanner M.F., Belew R.K., Goodsell D.S. and Olson A.J., AutoDock4 and AutoDockTools4: Automated docking with selective receptor flexibility, *Journal of Computational Chemistry*, **30**, 2785–2791 **(2009)**

23. Parackova Z., Milota T., Vrabcova P., Smetanova J., Svaton M., Freiberger T., Kanderova V. and Sediva A., Novel XIAP mutation causing enhanced spontaneous apoptosis and disturbed NOD2 signalling in a patient with atypical adult-onset Crohn's disease, *Cell Death & Disease*, **11**, 1–11 **(2020)**

24. Pavithra M.K.S., Procedure for chromatography using mobile phase with high elution strength to recover tacrolimus from the fermentation broth, *Res. J. Biotech*., **27(1)**, 71–77 **(2023)**

25. Pemmaraju N., Carter B.Z., Bose P., Jain N., Kadia T.M., Garcia-Manero G., Bueso-Ramos C.E., DiNardo C.D., Bledsoe S., Daver N.G., Popat U., Konopleva M.Y., Zhou L., Pierce S., Estrov Z.E., Borthakur G.M., Ohanian M., Qiao W., Masarova L., Wang X., Mak P.Y., Cortes J., Jabbour E. and Verstovsek S., Final results of phase 2 clinical trial of LCL161, an oral SMAC mimetic for patients with myelofibrosis, *Blood Advances*, **5**, 3163–3173 **(2021)**

26. Ponder J.W. and Richards F.M., Tertiary templates for proteins: Use of packing criteria in the enumeration of allowed sequences for different structural classes, *Journal of Molecular Biology*, **193**, 775–791 **(1987)**

27. Priya Doss C.G., Chakraborty C., Chen L. and Zhu H., Integrating In Silico Prediction Methods, Molecular Docking and Molecular Dynamics Simulation to Predict the Impact of ALK Missense Mutations in Structural Perspective, *BioMed Research International*, **2014**, 1–14 **(2014)**

28. Tian W., Chen C., Lei X., Zhao J. and Liang J., CASTp 3.0: computed atlas of surface topography of proteins, *Nucleic Acids Research*, **46**, W363–W367 **(2018)**

29. Tu H. and Costa M., XIAP's Profile in Human Cancer, *Biomolecules*, **10**, 1493 **(2020)**

30. UniProt Consortium, UniProt: a hub for protein information, *Nucleic Acids Research*, **43**, D204-212 **(2015)**

31. Weigelt J., Structural genomics-impact on biomedicine and drug discovery, *Experimental Cell Research*, **316**, 1332–1338 **(2010)**

32. Wu J.C., Chao E., Bier L.H. and Duckett C.S., Upstream regulatory role for XIAP in receptor-mediated apoptosis, *Molecular and Cellular Biology*, **24**, 7003-7014 **(2004)**

33. Yang L., Booth C., Speckmann C., Seidel M.G., Worth A.J.J., Kindle G., Lankester A.C., Grimbacher B., Sediva A., Neven B., Hauck F., Warnatz K., Pac M., Carrabba M., Palacin P., Jandus P., Gardulf A., Mahlaoui N., Pergent M., Schutz C., Sharapova S., Vassilios L., Candotti F., Volpi S., Gennery A.R., Seppanen M.R.J., Morris E.C. and Burns S.O., Phenotype, genotype, treatment and survival outcomes in patients with X-linked inhibitor of apoptosis deficiency, *Journal of Allergy and Clinical Immunology*, **150**, 456–466 **(2022)**

34. Zeissig Y., Petersen B.S., Milutinovic S., Bosse E., Mayr G., Peuker K., Hartwig J., Keller A., Kohl M., Laass M.W., Billmann-Born S., Brandau H., Feller A.C., Röcken C., Schrappe M., Rosenstiel P., Reed J.C., Schreiber S., Franke A. and Zeissig S., XIAP variants in male Crohn's disease, *Gut*, **64**, 66–76 **(2015)**

35. Zhang M., Wu K., Wang M., Bai F. and Chen H., CASP9 As a Prognostic Biomarker and Promising Drug Target plays a Pivotal Role in Inflammatory Breast Cancer, *International Journal of Analytical Chemistry*, **2022**, 1043445 **(2022)**

36. Zhou T., Parillon L., Li F., Wang Y., Keats J., Lamore S., Xu Q., Shakespeare W., Dalgarno D. and Zhu X., Crystal structure of the T315I mutant of AbI kinase, *Chemical Biology & Drug Design*, **70**, 171–181 **(2007)**.

(Received 12th February 2025, accepted 18th April 2025)